

Twin image elimination in digital holography by combination of Fourier transformations

Debesh Choudhury · Gautam Lohar

Abstract We present a new technique for removing twin image in in-line digital Fourier holography using a combination of Fourier transformations. Instead of recording only a Fourier transform hologram of the object, we propose to record a combined Fourier transform hologram by simultaneously recording the hologram of the Fourier transform and the inverse Fourier transform of the object with suitable weighting coefficients. Twin image is eliminated by appropriate inverse combined Fourier transformation and proper choice of the weighting coefficients. An optical configuration is presented for recording combined Fourier transform holograms. Simulations demonstrate the feasibility of twin image elimination. The hologram reconstruction is sensitive to phase aberrations of the object, thereby opening a way for holographic phase sensing.

Keywords Holographic twin image, in-line digital holography, combined Fourier transform.

1 Introduction

Twin image is an age old problem in holography since its invention by Gabor [1]. In 1951, Bragg and Rogers first eliminated the unwanted twin image by recording two holograms and doubling the object-to-hologram distance in between the exposures [2]. A nice review details several available techniques for getting rid of the twin image [3]. The off-axis holography of Leith and Upatnieks is the simplest method, but it requires high resolution recording materials [4]. Most other methods [3] either used optical/digital spatial filtering, or needed to record multiple phase shifted holograms, or utilized iterative reconstruction of the holograms

Debesh Choudhury

Department of Electronics and Communication Engineering

Neotia Institute of Technology, Management and Science

PO - Amira, D. H. Road, South 24 Parganas, Pin 743368, West Bengal, India

E-mail: debesh[AT]iitbombay[DOT]org

Gautam Lohar

Department of Electronics and Communication Engineering, JIS College of Engineering

Block A, Phase III, Kalyani, Nadia, Pin 741235, West Bengal, India.

thereby making the recording and/or reconstruction process slow. We propose to surmount this problem by recording a combined Fourier transform hologram and its computer reconstruction by inverse combined Fourier transformation.

2 Combination of Fourier transformations

If $g(x, y)$ is an object function, its forward Fourier transform (FT), i.e., $\mathcal{FT}\{g(x, y)\}$, is given by

$$\int_{-\infty}^{+\infty} \int_{-\infty}^{+\infty} g(x, y) \exp\{-i2\pi(ux + vy)\} dx dy = G(u, v) \quad (1)$$

and its inverse FT, i.e., $\mathcal{IFT}\{g(x, y)\}$, is given by

$$\int_{-\infty}^{+\infty} \int_{-\infty}^{+\infty} g(x, y) \exp\{i2\pi(ux + vy)\} dx dy = G^*(u, v) \quad (2)$$

where x, y and u, v are the space and spatial frequency coordinates pairs, $i = \sqrt{-1}$, \mathcal{FT} , \mathcal{IFT} signify Fourier transform and inverse Fourier transform operator and the symbol \star stands for complex conjugation. Following the definitions of FT and inverse FT, the identities below also hold

$$\mathcal{IFT}\{g(x, y)\} = G^*(u, v) = G(-u, -v) \quad (3)$$

$$\mathcal{IFT}\{g(-x, -y)\} = G^*(-u, -v) = G(u, v) \quad (4)$$

We now define a combined Fourier transform (CFT) as [5]

$$\begin{aligned} G_{cft}(u, v) &= a_1 \mathcal{FT}[g(x, y)] + a_2 \mathcal{IFT}[g(x, y)] \\ &= a_1 G(u, v) + a_2 G(-u, -v) \end{aligned} \quad (5)$$

where a_1 and a_2 are two constant coefficients, real or complex, but must satisfy $a_1^2 \neq a_2^2$. The object function $g(x, y)$ can be recovered by an inverse CFT (ICFT) given by

$$\begin{aligned} g(x, y) &= (a_1^2 - a_2^2)^{-1} [a_1 \mathcal{IFT}\{G_{cft}(u, v)\} \\ &\quad - a_2 \mathcal{FT}\{G_{cft}(u, v)\}] \end{aligned} \quad (6)$$

3 Combined FT Hologram recording

We record a CFT hologram by adding a coherent plane wave to the wave field distribution of equation (5). If R is the amplitude of the collimated reference wave, the wave field distribution at the hologram recording plane will be given by

$$\Psi(u, v) = R + G_{cft}(u, v) \quad (7)$$

The recorded hologram intensity will be given by

$$\begin{aligned} I(u, v) &= |\Psi(u, v)|^2 \\ &= |R|^2 + |G_{cft}|^2 + R G_{cft}^* + R^* G_{cft} \end{aligned} \quad (8)$$

The amplitude of the reference wave R is made large enough so as to make the hologram recording linear. We also capture a separate record of the reference wave intensity $|R|^2 = R^2$ only, prior to recording the combined Fourier transform hologram. Subtracting R^2 from both sides of equation (8) and also dividing both sides by R^2 , we get the modified hologram intensity as

$$I' = \frac{|G_{cft}|^2}{R^2} + \frac{1}{R^2} \{RG_{cft}^* + R^*G_{cft}\} \quad (9)$$

Since, $|R|^2 \gg |G_{cft}|^2$, $|G_{cft}|^2/|R|^2$ is vanishingly small, hence it can be neglected and equation (9) reads

$$I' \approx \frac{1}{|R|^2} \{RG_{cft}^* + R^*G_{cft}\} \quad (10)$$

4 Object reconstruction from the combined FT hologram

The object function $g(x, y)$ can be reconstructed from the CFT hologram by illuminating the hologram by the reference wave R and by ICFT operation, i.e.,

$$\mathcal{ICFT}[RI'] = \mathcal{ICFT}[G_{cft}^*] + \mathcal{ICFT}[G_{cft}] \quad (11)$$

since $R^*/R = 1$ because $R^* = R$, and \mathcal{ICFT} stands for ICFT operator. Using the identities of equations (3) and (4) and expanding the inverse CFTs, equation (11) can be expressed as

$$\mathcal{ICFT}[RI'] = A_1g(x, y) + A_2g(-x, -y) \quad (12)$$

where A_1 and A_2 are constants involving the weighting coefficients a_1 and a_2 given by

$$A_1 = \left(1 + \frac{a_1a_2^* - a_1^*a_2}{|a_1|^2 - |a_2|^2}\right), \quad A_2 = \left(\frac{a_1a_1^* - a_2a_2^*}{|a_1|^2 - |a_2|^2}\right) \quad (13)$$

If we take values of a_1 and a_2 such that they are mutually complex conjugate, as for example, if

$$a_1 = b_1 + ib_2 \quad \text{and} \quad a_2 = b_1 - ib_2 \quad (14)$$

b_1 and b_2 being real, $A_1 = 1$ but $A_2 = 0$, and equation (12) reads

$$\{\mathcal{ICFT}[RI']\}_{a_1=a_2^*} = g(x, y) \quad (15)$$

That means, only the object function $g(x, y)$ is reconstructed and the conjugate reconstruction $g(-x, -y)$ is eliminated. If a_1 and a_2 are not exactly complex conjugates of each other, the twin image will be present. The strengths of the two images will depend on the real and imaginary parts of a_1 and a_2 .

By De Moivre's theorem, equation (14) can be expressed as

$$a_1 = B \exp(i\phi) \quad \text{and} \quad a_2 = B \exp(-i\phi) \quad (16)$$

$$\text{where } B = \sqrt{b_1^2 + b_2^2} \quad \text{and} \quad \phi = \tan^{-1}(b_2/b_1) \quad (17)$$

Putting a_1 and a_2 , equation (5) becomes

$$\begin{aligned} G_{cft}(u, v) &= B\{\exp(i\phi)G(u, v) \\ &\quad + \exp(-i\phi)G(-u, -v)\} \\ &= B \exp(-i\phi)\{\exp(i2\phi)G(u, v) + G(-u, -v)\} \end{aligned} \quad (18)$$

i.e., $g(-x, -y)$. A third Fourier lens FL_3 is also placed which produces the Fourier transforms of $g(x, y)$ and $g(-x, -y)$ with appropriate coefficients that depend on the phase relationship between the wave fields propagating through the interferometric arms. The orientations of the polarizing components are shown in a dashed box. Another part of the input beam from the laser, which is transmitted from the beam-splitter BS_1 and is reflected by the mirror M_3 , superposes with object bearing beams after transmitting through another beam-splitter BS_2 . To get a CFT hologram at the CCD plane, the phase differences between the beams are adjusted to 2ϕ using polarization-induced phase [6].

The input laser beam is polarized by the polarizer P_1 at angle $\pi/4$ to the x -axis, and may be represented by a Jones vector \hat{E} as [7]

$$\hat{E} = E_0 \begin{bmatrix} 1 \\ 1 \end{bmatrix} \quad (19)$$

E_0 being the amplitude. This polarized beam is split by the polarizing beam-splitter PBS into two orthogonally polarized beam along the x -axis and y -axis, and the Jones matrices corresponding to the PBS along the x -axis and y -axis may be given by [7]

$$P_x = \begin{bmatrix} 1 & 0 \\ 0 & 0 \end{bmatrix}, \quad P_y = \begin{bmatrix} 0 & 0 \\ 0 & 1 \end{bmatrix} \quad (20)$$

The reflected polarized beam, after a round trip through the cyclic interferometer gets reflected by the PBS and comes out at the output side. Similarly, the transmitted polarized component comes out of the PBS by transmission at the output side. It is to be noted that these two polarized beams carry the object transmittance information $g(x, y)$ and its inversion $g(-x, -y)$ by appropriate lens transformation inside the interferometer. These two orthogonally polarized image bearing beams face a quarter-wave retardation plate QWP whose slow axis makes an angle $\pi/4$ with the x -axis. Finally, these two polarized beams after passing through the quarter-wave plate will pass through an analyzer P_2 and the wave fields proceed towards the CCD camera. After Fourier transformation by the third lens, the vector wave field distribution at the CCD camera plane will be given by

$$\begin{aligned} \hat{G}_{PI}(u, v) = & P(\theta)[C(\pi/4)P_x\hat{E}G(u, v) \\ & + C(\pi/4)P_y\hat{E}G(-u, -v)] \end{aligned} \quad (21)$$

where $P(\theta)$ represents the Jones matrix of the analyzer P_2 , $C(\pi/4)$ represents the Jones matrix of the quarter-wave retardation plate, and are given by [7]

$$P(\theta) = \begin{bmatrix} \cos^2 \theta & \cos \theta \sin \theta \\ \sin \theta \cos \theta & \sin^2 \theta \end{bmatrix} \quad (22)$$

$$C(\pi/4) = \frac{1}{2} \begin{bmatrix} 1+i & 1-i \\ 1-i & 1+i \end{bmatrix} \quad (23)$$

Performing matrix multiplications, equation (21) can be expressed as

$$\begin{aligned} \hat{G}_{PI}(u, v) = & \left[\exp \left\{ i \left(\frac{\pi}{4} - \theta \right) \right\} G(u, v) + \exp \left\{ -i \left(\frac{\pi}{4} - \theta \right) \right\} G(-u, -v) \right] \\ & \times \begin{bmatrix} \cos \theta \\ \sin \theta \end{bmatrix} \end{aligned} \quad (24)$$

where we have dropped off the constant amplitude factors. If we put $\theta = \pi/4 - \phi$, the polarization-induced phase difference becomes 2ϕ , and equation (24) becomes equivalent to the field distribution given by equation (18) and is nothing but the CFT of the object function $g(x, y)$ except that it is linearly polarized. We can also identify the phase factors $\exp\{i(\pi/4 - \theta)\}$ and $\exp\{-i(\pi/4 - \theta)\}$ as the complex coefficients a_1 and a_2 respectively.

Finally, an analyzer P_3 should be placed before the CCD camera whose transmission axis makes an angle θ (same as P_2) with the x -axis. A half-wave plate HWP should also be placed after the Fourier lens FL_3 with its slow axis making an angle α ($\alpha \neq \theta$) with the x -axis, so as to keeping the amplitudes of the object waves reaching the CCD camera much smaller than the amplitude of the reference wave. This will help to ensure that $|R|^2 \gg |G_{cft}|^2$. The object waves and the reference wave will transmit through the analyzer P_3 and interfere to form the CFT hologram which can be recorded by the CCD camera.

6 Feasibility Simulations

Although the derivations of the earlier sections are shown for continuous combined Fourier transform, it can be shown that the results are valid for discrete combined Fourier transform as well. We have carried out proof-of-the-principle study using computer simulations by using GNU Octave [8]. The object transparency is of 200x200 pixels size as shown in Fig.2(a). The simulation window size is 256x256 pixels where the 200x200 pixels object is placed at the right hand top corner with zero padding. The object is purposefully off-centered so as to distinguish the twin reconstructions. The computational reconstruction of the object from a discrete FT hologram is carried out and is shown in Fig.2(b). Simulations for object reconstructions from the discrete CFT hologram can be done for two cases: Case I considering real object, and Case II considering complex object.

6.1 Case I: Reconstruction with a real object

This case is straight forward. Computational reconstructions from simulated discrete CFT holograms for different values of a_1 and a_2 are shown in Fig.2(c) and 2(d) for $a_1 \approx a_2^*$ ($b_1 = 1.7, b_2 = 1$) and for $a_1 = a_2^*$ ($b_1 = b_2 = 1$) respectively. It is evident from Fig.2(b) that reconstruction of the FT hologram reproduces twin image with equal strengths. On the otherhand, for the CFT hologram, the effect of twin image is present for $a_1 \neq a_2^*$ ($b_1 = 1.7, b_2 = 1$), but the intensity levels of the two images are unequal [Fig.2(c)]. The effect of twin image is completely eliminated for $a_1 = a_2^*$ ($b_1 = b_2 = 1$) as discernible from Fig.2(d). It is clear from the results of Fig.2(c) and Fig.2(d) that the effects of twin image in reconstructions of CFT holograms can be controlled by proper choice of a_1 and a_2 , and can be completely eliminated for $a_1 = a_2^*$.

6.2 Case II: Reconstruction with a complex object

In practical situation the object would generally be complex, because the object transparency (either on glass plate or film) would have a phase variation due to

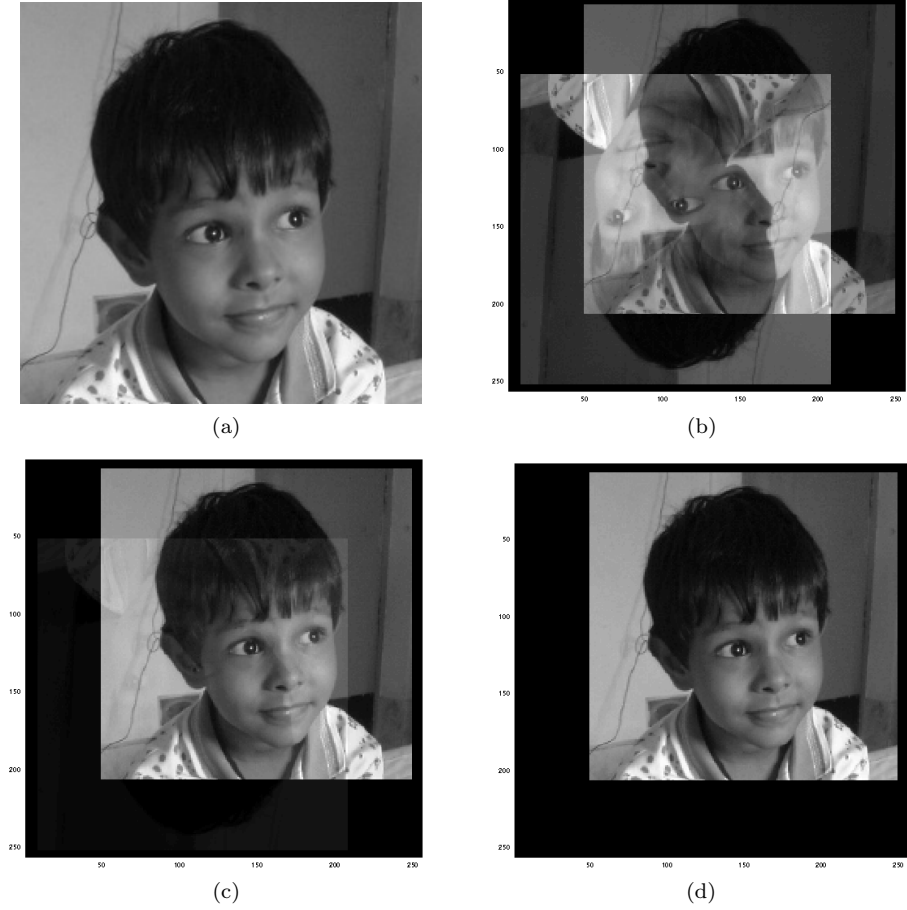


Fig. 2 Simulation results with a real object: (a) Object; Reconstruction from (b) FT hologram, (c) CFT hologram with $a_1 \approx a_2^*$, and (d) CFT hologram with $a_1 = a_2^*$.

variation in thickness or refractive index of the material or both. If $t(x, y)$ represents the thickness distribution over the object transparency, the phase distribution due to this thickness variation will be given by

$$\delta(x, y) = n \left(\frac{2\pi}{\lambda} \right) t(x, y) \quad (25)$$

where λ is the wavelength of the laser and n is the refractive index of the material of the transparency. Here, it is assumed that the refractive index of the material of the object transparency is uniform. We consider an example of a quadratic thickness variation, so $t(x, y)$ may be expressed as

$$t(x, y) = t_0 + (x^2 + y^2)\Delta \quad (26)$$

where t_0 is the constant nominal thickness of the transparency plate and Δ is a thickness that is varied quadratically with spatial coordinates x, y . Therefore, the

effect will be a phase factor $\exp[i\delta(x,y)]$ multiplied to the object function. If we put $\Delta = 0$, we get a constant phase factor which is equivalent to the real object of Case I.

Simulations have been carried out with a 200x200 size phase function multiplied with the 200x200 size object function for $\lambda = 633$ nm, $t_0 = 2$ mm and different values of Δ , the overall simulation window remaining 256x256 size. The surface plot of the normalized phase function $t(x,y)$ for $\Delta = 0$, and $\Delta = 0.5\lambda$ are shown in Fig.3(a) and 3(b). The phase function profile is constant in Fig.3(a) which is nothing but the case of real object of Case I. The computational reconstructions of CFT holograms are shown in Fig.3(c), 3(d), 3(e) and 3(f) for $\Delta = 0, 0.5\lambda, \lambda$ and 2λ respectively. Here, the weighting multipliers are kept at $a_1 = a_2^*$ and $b_1 = b_2 = 1$ for all. It is evident from Fig.3(c) – 3(f) that the phase variation of the object transparency gives rise to circular fringes modulated over the reconstructed object image. The effect is negligible for $\Delta = 0.5\lambda$ [Fig.3(d)], but as Δ increases to λ , a circular fringe appears near the periphery of the image [Fig.3(e)]. When $\Delta = 2\lambda$, the image is modulated by two circular fringes [Fig.3(f)]. It is clear that the thickness of the object transparency should be optically uniform, i.e., the surface finish of the object transparency plays an important role. That is why in such an interferometric arrangement, the object transparency may be placed inside an optical tank filled with an index matching liquid and optically polished glass windows with surface finish better than $\lambda/4$.

7 Discussions

The proof-of-the-principle simulations of the previous section proved the feasibility of twin image elimination in digital in-line holography using CFT. The proposed system is a polarization triangular path interferometer with a couple of Fourier lenses for synthesizing an inversion of the object function $[g(-x, -y)]$, along with the object function $[g(x, y)]$, and another Fourier lens for performing Fourier transform of the object and its inversion. The effect of CFT is created by introducing appropriate phase difference between the object information bearing waves by a polarization technique. Simulation is carried out for generating the CFT holograms for different values of the complex weighting factors. In this simulation, we have not considered the practical aspects of experimentation, such as effects of imperfections of the polarization components, aberrations of the Fourier lenses and the mirrors, misalignment errors of the interferometer, object wave to reference wave ratios and the quantization errors of the CCD camera.

The alignment of the proposed interferometric system is not easy, nevertheless it is possible to implement combined Fourier transform optically. From equations (16), (17) and (18) it is evident that the complex constants a_1 and a_2 are transformed into a phase difference 2ϕ . So, in optical implementation, the constants a_1 and a_2 are not required to be specified directly, instead the orientations of the polarizing components are so adjusted such that the phase difference 2θ between the two image bearing object waves can be made equal to 2ϕ . If one desires, one can easily express the induced phase differences equivalent to the complex factors a_1 and a_2 using De Moivre's relations of equations (16) and (17). The complex coefficients a_1 and a_2 are also identified in the output of the interferometer in equation (24) as exponential phase factors.

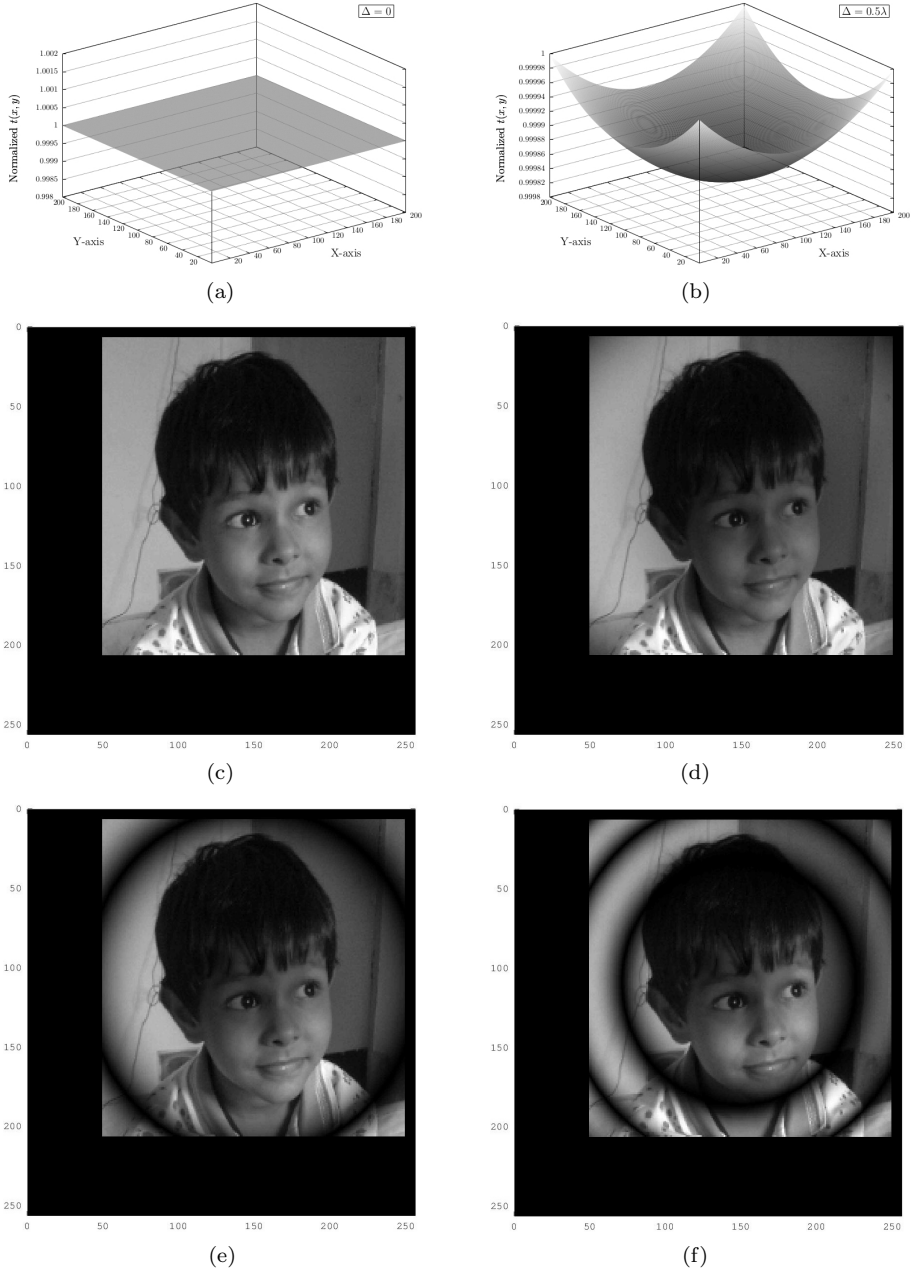


Fig. 3 Simulation results with a complex object: The normalized phase function $t(x, y)$ is shown for (a) $\Delta = 0$ and (b) $\Delta = 0.5\lambda$. Reconstructions from the CFT hologram are shown for (c) $\Delta = 0$, (d) $\Delta = 0.5\lambda$, (e) $\Delta = \lambda$ and (f) $\Delta = 2\lambda$.

Since, it is an interferometric transformation, the holographic reconstruction is sensitive to phase aberrations of the object transparency. Thus, this technique may be useful for carrying out studies of phase objects. A similar inverting triangular path polarization interferometer was indeed utilized for implementing optical Hartley transform experimentally [9]. We wish to consider the practical aspects in a future experimental implementation of the proposed method.

8 Conclusion

We have proposed a technique for resolving twin image problem of in-line digital Fourier holography. We use a combination of Fourier transforms to eliminate the unwanted twin image. The technique relies on interferometric addition of Fourier transforms of the object and its inversion with appropriate complex weighting coefficients, which are introduced through polarization-induced phase. Simulation results prove the feasibility of complete elimination of one of the twin image. Moreover, the technique is sensitive to phase aberrations of the object transparency, thereby providing a way for phase sensing holographic imaging. The proposed method neither involves recording of several phase shifted holograms, nor it requires any iteration for digital reconstruction, which may render it suitable for recording holograms of fast changing sequences as well as fast digital reconstruction of the recorded holograms.

Acknowledgements The authors thank an anonymous reviewer for fruitful comments that helped to improve the paper.

References

1. D. Gabor, "A new microscopic principle," *Nature* **161**, 777-778 (1948).
2. W. L. Bragg and G. L. Rogers, "Elimination of the unwanted image in diffraction microscopy," *Nature* **167**, 190 (1951).
3. B. M. Hennelly, D. P. Kelly, N. Pandey, D. Monaghan, "Review of twin reduction and twin removal techniques in holography," *Proc. China-Ireland International Conference on Information and Communications Technologies*, Maynooth, Ireland, Pages 241-245 (2009).
4. E. Leith and J. Upatnieks, "Wavefront reconstruction with continuous-tone objects," *JOSA* **53** 1377-1381 (1963).
5. R. Ansari, "An extension of the discrete Fourier transform," *IEEE Trans Circuits Sys. CAS-32* (6), 618-619 (1985).
6. D. Choudhury, P. N. Puntambekar and A. K. Chakraborty, "Utilization of polarization-induced phase difference for complex addition and subtraction of amplitudes," *J. Opt.* **22**, 6-10 (1993).
7. A. Gerald and J.M. Burch, *Introduction to Matrix Methods in Optics* (John Wiley & Sons, 1975).
8. GNU Octave: <http://www.gnu.org/software/octave/> (accessed December 4, 2012)
9. D. Choudhury, P. N. Puntambekar and A. K. Chakraborty, "Hartley transformation by an inverting interferometer," *J. Opt.* **26** (1997) 139-145.